nature materials

ARTICLES

https://doi.org/10.1038/s41563-022-01281-7

Subsecond multichannel magnetic control of select neural circuits in freely moving flies

Charles Sebesta[1], Daniel Torres Hinojosa[1], Boshuo Wang[2], Joseph Asfouri[3], Zhongxi Li[4], Guillaume Duret[3], Kaiyi Jiang[1,5], Zhen Xiao[6], Linlin Zhang[1], Qingbo Zhang[1], Vicki L. Colvin[6], Stefan M. Goetz[2,4,7,8,9], Angel V. Peterchev[2,4,7,10], Herman A. Dierick[11,12], Gang Bao[1] and Jacob T. Robinson[1,3,12] ✉

Precisely timed activation of genetically targeted cells is a powerful tool for the study of neural circuits and control of cell-based therapies. Magnetic control of cell activity, or 'magnetogenetics', using magnetic nanoparticle heating of temperature-sensitive ion channels enables remote, non-invasive activation of neurons for deep-tissue applications and freely behaving animal studies. However, the in vivo response time of thermal magnetogenetics is currently tens of seconds, which prevents precise temporal modulation of neural activity. Moreover, magnetogenetics has yet to achieve in vivo multiplexed stimulation of different groups of neurons. Here we produce subsecond behavioural responses in *Drosophila melanogaster* by combining magnetic nanoparticles with a rate-sensitive thermoreceptor (TRPA1-A). Furthermore, by tuning magnetic nanoparticles to respond to different magnetic field strengths and frequencies, we achieve subsecond, multichannel stimulation. These results bring magnetogenetics closer to the temporal resolution and multiplexed stimulation possible with optogenetics while maintaining the minimal invasiveness and deep-tissue stimulation possible only by magnetic control.

Magnetic stimulation of genetically targeted cells, or magnetogenetics, may enable researchers to apply a magnetic stimulus throughout the brain of a freely moving animal in a non-invasive manner to study circuits that are deep within the brain or distributed over large areas. One approach of magnetogenetics with well-described physical phenomena relies on the presence of two components in the tissue: (1) synthetic magnetic nanoparticles that convert alternating magnetic fields into heat and (2) thermoreceptors that convert local heat into neural activity[1–3]. While there have been reports of magnetogenetic technologies that rely on purely genetically encoded proteins[4–7], it is currently unclear how these magnetically sensitized chimeric proteins function[8,9].

Compared with optical methods for stimulation of genetically targeted cells (optogenetics)[10,11], magnetogenetics offers unique advantages for deep volumetric targets. While optogenetics has response times of 10–20 ms (ref. [12]), most optical wavelengths are effective only at distances of a few millimetres from an optical source due to tissue scattering. In contrast, magnetic fields in the frequency range 0.1–1.0 MHz have very low attenuation in bone, air and biological tissue[13]. This superior bone and tissue penetration of magnetic fields eliminates the need for invasive surgeries to introduce the light probes typically required for optogenetic stimulation, interventions that can cause potential tissue damage from implantation and heat generation.

While magnetogenetics offers advantages, including deep-tissue volumetric stimulation and minimal invasiveness, the reported in vivo response time of magnetogenetic technologies is in the order of 10 s—more than 1,000-fold slower than optogenetic stimulation, largely due to the thermoreceptors used. Previous experiments with membrane-targeted, cobalt-doped nanoparticles have shown latencies of 2.18 ± 0.17 s in *trpV1*$^+$ neurons in vitro and 22.8 ± 2.6 s in vivo via motor cortex stimulation, resulting in an ambulatory response in *trpV1*$^+$ mice[2]. Earlier experiments with undoped iron oxide nanoparticles showed a ~5 s latency in vitro with *trpV1*$^+$ neurons, with upregulation of c-Fos expression in vivo in the order of minutes[3]. Existing magnetogenetic methods rely on thermoreceptors (for example, TRPV1) that respond at temperatures several degrees above body temperature, but heating the surrounding tissue to the threshold response temperature can take several seconds. These multisecond latencies prevent precise timing with behavioural or environmental cues that are essential for studying the relationship between neural activity and behaviour. Magnetic activation of mechanoreceptors in contact with magnetic particles that move in response to a magnetic field offers a path to faster stimulation[14], but the in vivo response time remains in the order of several seconds and requires micrometre-sized particles or aggregates that can be difficult to deliver in vivo[15].

In this work we replaced threshold thermoreceptors with a rate-sensitive thermoreceptor to achieve subsecond response times approaching what can be achieved with optogenetics. Since magnetic nanoparticle heating can increase tissue temperature rapidly, the use of thermal rate sensors eliminates the wait time required for tissue to reach a threshold activation temperature when using thermoreceptors like TRPV1. Recent work demonstrates that

[1]Department of Bioengineering, Rice University, Houston, TX, USA. [2]Department of Psychiatry & Behavioral Sciences, School of Medicine, Duke University, Durham, NC, USA. [3]Department of Electrical and Computer Engineering, Rice University, Houston, TX, USA. [4]Department of Electrical and Computer Engineering, School of Engineering, Duke University, Durham, NC, USA. [5]Department of Biological Engineering, Massachusetts Institute of Technology, Cambridge, MA, USA. [6]Department of Chemistry, Brown University, Providence, RI, USA. [7]Department of Neurosurgery, School of Medicine, Duke University, Durham, NC, USA. [8]Institute of Brain Sciences, Duke University, Durham, NC, USA. [9]Department of Engineering, School of Technology, University of Cambridge, Cambridge, UK. [10]Department of Biomedical Engineering, School of Engineering, Duke University, Durham, NC, USA. [11]Department of Molecular and Human Genetics, Baylor College of Medicine, Houston, TX, USA. [12]Department of Neuroscience, Baylor College of Medicine, Houston, TX, USA. ✉e-mail: JTRobinson@rice.edu

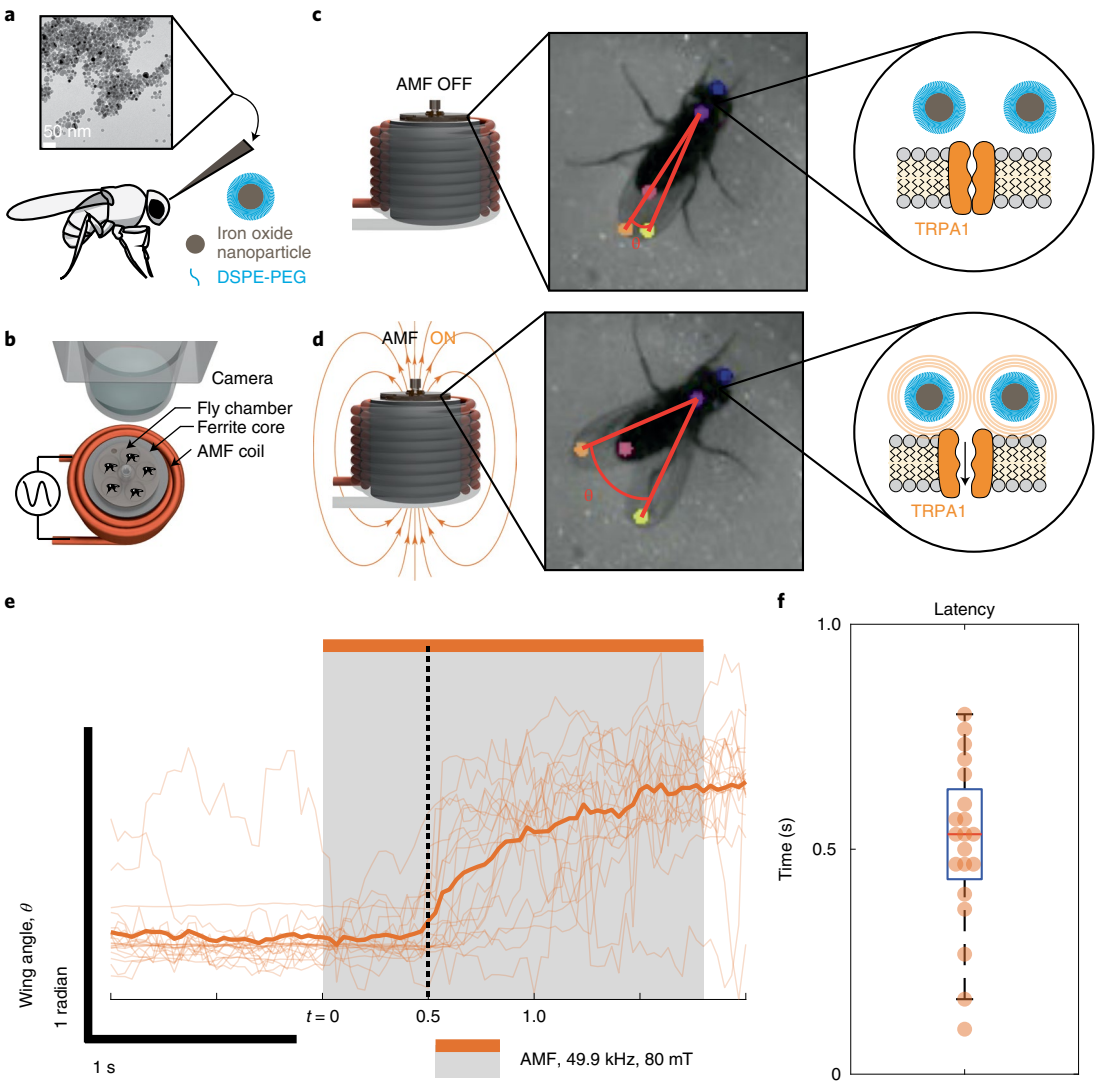

Fig. 1 | Behavioural fly assay. a, TEM image and schematic of nanoparticle injection between ocelli. **b**, Freely moving flies in behaviour chambers remotely stimulated by an induction coil and monitored by camera for simultaneous comparison of multiple individuals. **c**, Left, placement of the behaviour chamber on top of the magnetic coil with a ferrite core. Middle, flies were imaged at 30 frames s^{-1} to enable automatic posture estimation, annotated by DeepLabCut. Right, schematic of nanoparticles in close proximity to TRPA1 channels. **d**, AMF activation of the coil (left) resulted in wing-opening response (middle) due to TRPA1-A channel activation by hysteretic heating of nearby nanoparticles (right). **e**,**f**, Flies showed distinct and reversible neuronal activation of cells expressing *fruitless*, with subsecond behavioural responses repeatedly observed (**e**); average of $n = 5$ flies examined over four repeated AMF stimulations (49.9 kHz, 80 mT), with average behavioural response of 510 ± 186 ms (**f**, mean ± s.d.) as observationally determined by video (Supplementary Video 2). $n = 5$ flies examined over four AMF stimulations. For the box plot, the centre line represents the median with bottom and top edges of the box representing 25th and 75th percentiles and whiskers extending to extreme data points not considered as outliers.

Drosophila TRPA1-A is activated by subtle temperature changes for temperature avoidance[16]. Additionally, this activation is susceptible to the rate of temperature change and rapid heating can lower the response threshold from ~34.5 to ~29.1 °C, potentially because of calcium-driven TRPA1 inactivation[17]. Additional experiments suggest that, when natively expressed in organs or tissues[18], TRPA1 is responsible for diverse sensitivity to temperature[19] with behavioural responses to changes of 0.01 °C in *Drosophila*[20], 0.005 °C in *Caenorhabditis elegans*[21] and 0.003 °C in snakes[22], making it an ideal target receptor to confer rapid, sensitive thermosensation. Therefore, we selected TRPA1-A as the thermoreceptor for optimization of magnetothermal channel activation and demonstration of subsecond, multichannel magnetogenetics in *Drosophila*. Since TRPA1-A is native, rate sensitive and commonly used for thermogenetics with genetic lines readily available, our approach can be applied to a wide range of magnetogenetic studies of brain function. *Drosophila* was used here to develop new magnetogenetic tools that can be adapted to other organisms. In larger animals, local heating of nanoparticles associated with rate-sensitive thermoreceptors can stimulate targeted cells without the surrounding tissues being affected by bulk heating. For this test bed, we chose to modulate two readily observable phenotypes by activation of cells expressing TRPA1 under the control of different drivers: (1) *fruitless*, resulting in wing extension and (2) Hb-9, resulting in side-to-side movement.

In vivo magnetogenetic activation of wing extension

To test whether the *Drosophila* TRPA1-A rate-sensitive thermoreceptor would indeed enable subsecond magnetogenetic activation, we developed a system to measure *Drosophila* behaviour under the influence of an alternating magnetic field (AMF). We generated fly

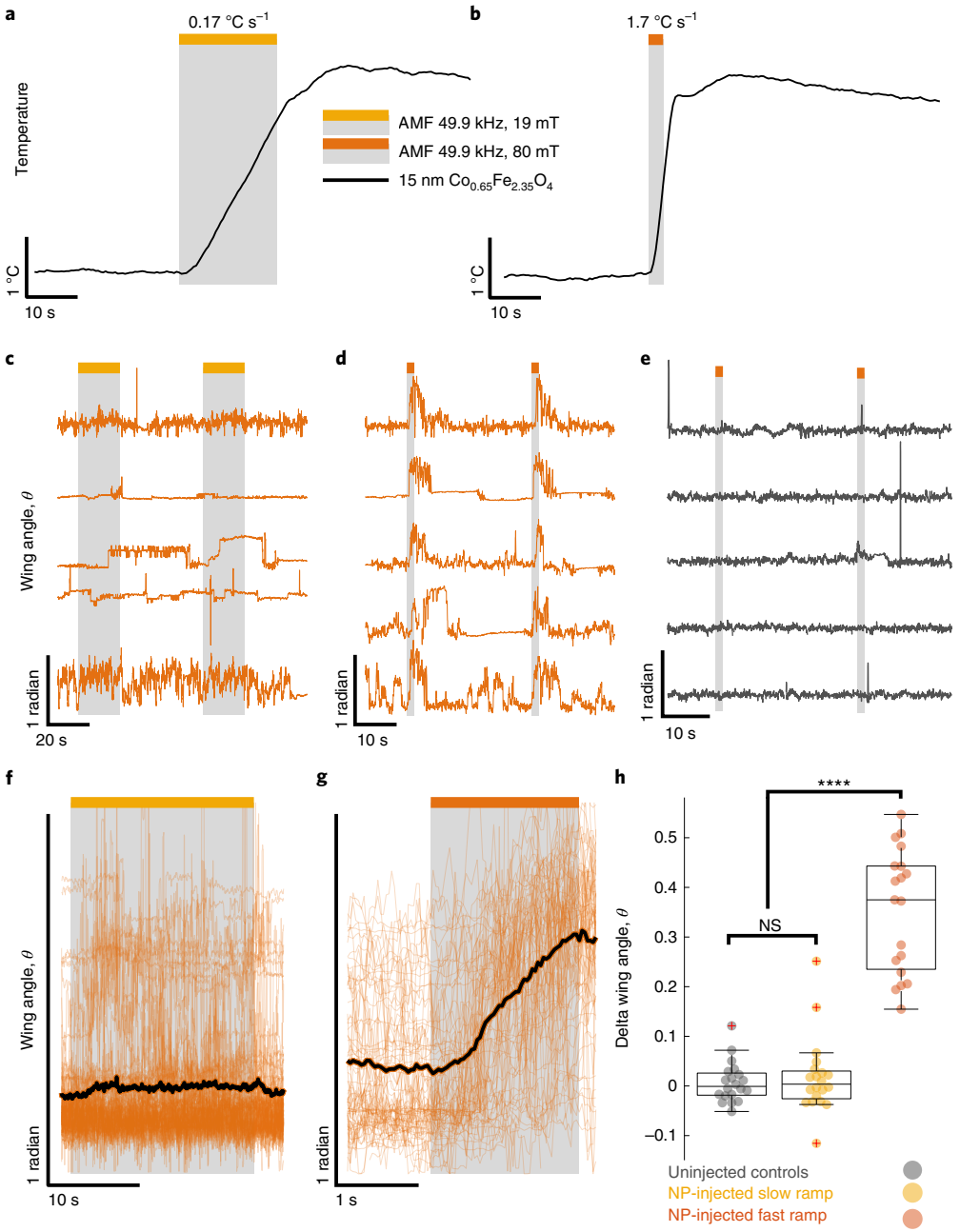

Fig. 2 | Rate response of magnetogenetic stimulation of cells expressing *fruitless* at subsecond response time. a,**b**, Thermal response of 15 nm cobalt-doped iron oxide nanoparticles at 10 mg ml^{-1} when exposed to AMF for (**a**) 20 s (49.9 kHz, 19 mT, shown in yellow) or (**b**) 1.8 s (49.9 kHz, 80 mT, shown in orange), reaching identical threshold temperature at rates of 0.17 and 1.7 °C s^{-1}, respectively. Visible lag in heat measurement is due to thermal resistance in the fiberoptic probe. **c**–**e**, Wing angle plots of the same five flies injected with 200 nl of 15 nm iron oxide nanoparticles (10 mg ml^{-1}) and expressing TRPA1 under the Fru-Gal4 driver when exposed to AMF for 20 s (49.9 kHz, 19 mT; **c**) or 1.8 s (49.9 kHz, 80 mT; **d**), and wing angle plots of uninjected flies exposed for 1.8 s (49.9 kHz, 80 mT; **e**). Stimulation experiments were repeated twice for each stimulation protocol for each set of five flies in the chamber (Supplementary Videos 1 and 2). **f**,**g**, Average traces of 20 flies, each responding to four repeated AMF stimulations with slow ramp (20 s, 49.9 kHz, 19 mT; **f**) or fast ramp (1.8 s, 49.9 kHz, 80 mT; **g**). **h**, One-way ANOVA of delta wing angle taken immediately before and after stimulation and compared with uninjected control flies (Supplementary Fig. 3) (****$P < 0.0001$; $P = 1.04 \times 10^{-9}$). $n = 20$ flies examined over four AMF stimulations. $P = 3.37 \times 10^{-19}$, $F = 99.9$, d.f. = 2. Post hoc analysis with Tukey's honest significant distance (HSD) test. Normal distribution for each group determined by Chi-square goodness-of-fit test. For the box plot, the centre line represents the median with bottom and top edges of the box representing 25th and 75th percentiles and whiskers extending to extreme data points not considered as outliers (Supplementary Videos 1 and 2). NS, not significant; NP, nanoparticles.

strains expressing thermal rate-sensitive TRPA1-A channels under the control of the *fruitless* driver, which is known to control courtship behaviour in males. Activation of cells expressing *fruitless* is readily observed by the lateral wing extension behavioural response, as previously shown with optogenetic[23,24] and thermogenetic[25] stimulation. Moreover, behaviour can be automatically tracked using pose estimation tools such as DeepLabCut[26] or FlyTracker[27] that eliminate observer bias. Rather than externally heating flies to activate the thermosensitive channel, we injected nanoparticles suspended in artificial *Drosophila* haemolymph (Fig. 1a, Supplementary

Fig. 1 and Methods). We placed the injected flies over an induction coil (Fig. 1b) and monitored wing-opening behaviour during AMF stimulation with a custom AMF generator[28]. The dissipated heat generated by the stimulated nanoparticles activates the dTRPA1-A protein channel (Fig. 1c,d).

When we injected flies with 10 μg ml^{-1} 15 nm cobalt-doped iron oxide nanoparticles and applied an AMF, we observed a rapid increase in wing angle with a response latency of 510 ± 186 ms observed from repeated stimulations on five flies—more than tenfold faster than previous in vivo magnetogenetic latencies[2,3] (Fig. 1e). Conversely, wing angle significantly decreased after ~370 ms and returned to baseline ~5.0 s after cessation of stimulation, as calculated from the average of traces collected from 20 flies (Supplementary Fig. 9). To confirm that the response was driven by magnetic heating of nanoparticles, we compared wing opening in flies injected with 19 nm of superparamagnetic iron oxide nanoparticles (SPIONs) with that in flies injected with 19 nm of low-specific loss power (-SLP) SPION particles (Supplementary Fig. 4). These low-SLP SPION particles contained the same amount of iron as the SPION particles, but are a mixture of wüstite and other iron oxidation states with a smaller hysteresis loop and thus do not heat well in an AMF[29,30], as characterized by alternating current (AC) magnetometry (Supplementary Fig. 5). When we applied an AMF to these flies, we observed a subsecond wing-opening response in iron oxide SPION-injected flies but no response in low-SLP SPION-injected flies, confirming that the behavioural response is mediated by magnetothermal heating (Supplementary Fig. 2 and Supplementary Videos 1 and 2), and no response in uninjected control flies (Supplementary Fig. 3).

Fast behavioural response via rate-sensitive thermoreceptors

By comparing the fly response to fast and slow heating rates, we were able to confirm that the wing-opening response is indeed regulated by the rate-sensitive properties of TRPA1 (ref. [17]). To perform behavioural experiments at different heating rates, we first characterized nanoparticle heating under two AMF conditions (49.9 kHz at field strengths of 80 or 19 mT). These different AMF conditions resulted in a ~tenfold difference in heating rate (Fig. 2a,b), calculated as averages over AMF duration due to visible lag from thermal resistance in the fiberoptic probe. To assess the rate sensitivity of adult fly behaviour, we exposed the same set of flies to different temperature ramps reaching roughly the same final temperature but over different periods of time. We achieved this by altering magnetic field strength for different durations of time (1.8 and 20 s, $\Delta T < 1.12$ °C; Methods). During these experiments we monitored wing angle responses of adult males expressing TRPA1-A, and plotted these data in Fig. 2c,d. The two heating conditions resulted in tissues reaching a similar maximum threshold temperature but at different rates (Fig. 2a,b), with sufficient sample size as determined by power analysis (Supplementary Fig. 8). The higher rate of temperature change ($\Delta T/t$) lowered the threshold temperature of the TRPA1 channels[17] and resulted in a statistically significant change in wing-opening phenotype (Fig. 2f–h) where ΔT is the temperature increase the fly is exposed to. Assuming similar thermal capacitance (C) for each fly, we expect all animals to receive the same total heat but at different rates ($\Delta T = \Delta Q/C$). Experiments conducted on standard controls and flies expressing the temperature-threshold-sensitive human TRPV1 channel showed no response. This further demonstrates the improved sensitivity achieved by the rate-sensitive TRPA1 channel (Supplementary Figs. 6 and 7).

Fast magnetogenetic activation of a second behaviour (Hb-9)

To generalize our findings, we also expressed the TRPA1 channel in an alternative neural circuit, producing a different behavioural

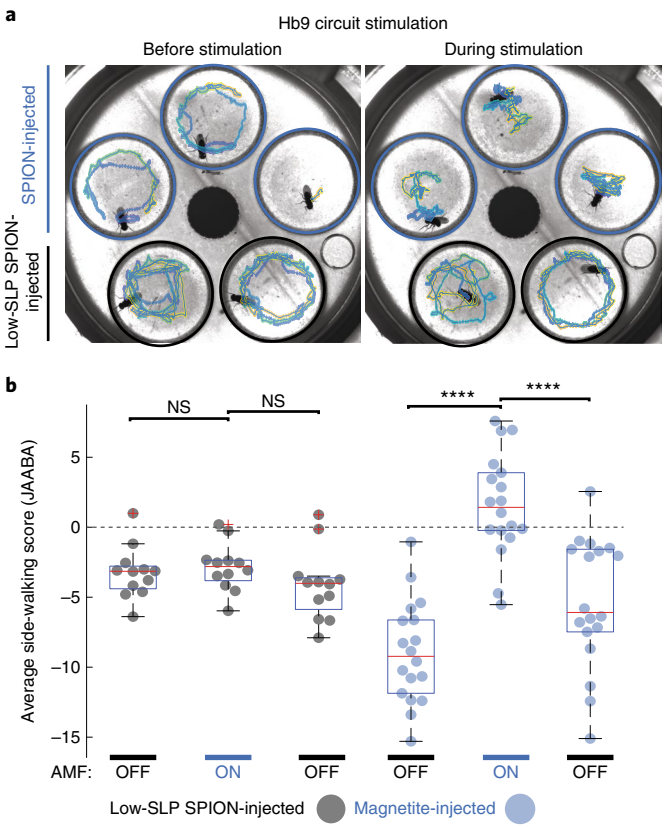

Fig. 3 | Versatility of magnetothermal stimulation in secondary cell type expressing Hb-9. a, Blue, flies injected with iron oxide SPION; black, controls injected with low-SLP SPION. Purple–yellow gradient traces show 20 s of fly trajectories immediately before AMF stimulation and 10 s after the start of magnetic stimulation (40 kA m^{-1} at 380 kHz). **b**, Box plot of average side-walking score from JAABA analysis of magnetic stimulation of flies expressing TRPA1 under the control of the Hb9 driver trained by exogenous thermal stimulation of flies with the same genotype. Positive scores indicate probable side-walking behaviour. Averages are taken over 20 s each immediately before stimulation, 10 s after the start of stimulation and 10 s after the end of stimulation. $n = 15$ flies (nine injected with SPION, six injected with low-SLP SPION. One-way ANOVA and Tukey's HSD test (****$P < 0.0001$); $P = 3.09 \times 10^{-12}$, $F = 18.28$, d.f. = 5 (Supplementary Video 3). For the box plot, the centre line represents the median with bottom and top edges representing the 25th and 75th percentiles and whiskers extending to extreme data points not considered as outliers.

effect. Driving the expression of *dTRPA1-A* with *Hb9-GAL4* reliably induced a side-walking phenotype[23] in the same behaviour chamber under AMF control (Fig. 3).

We observed a clear, robust and reversible side-walking phenotype during AMF stimulation among SPION-injected flies expressing *dTRPA1-A* under the control of the Hb-9 driver. In contrast, flies injected with poorly heating low-SLP SPIONs showed no response, demonstrating that behavioural responses are due to specific nanoparticle heating and not an artefact of magnetic field generation. The side-walking behaviour was more difficult to quantify than wing extension and took longer to develop. This increased latency may be due to the need to activate the peripheral nervous system where we would expect fewer nanoparticles. Nevertheless, magnetogenetic-driven behaviour was readily identified from the side-to-side behaviour tracks (Fig. 3a) and animal behaviour videos (Supplementary Video 3). FlyTracker generated a set of metrics for each track including wing angle, velocity, angular velocity and distance from the chamber wall. The combination of these

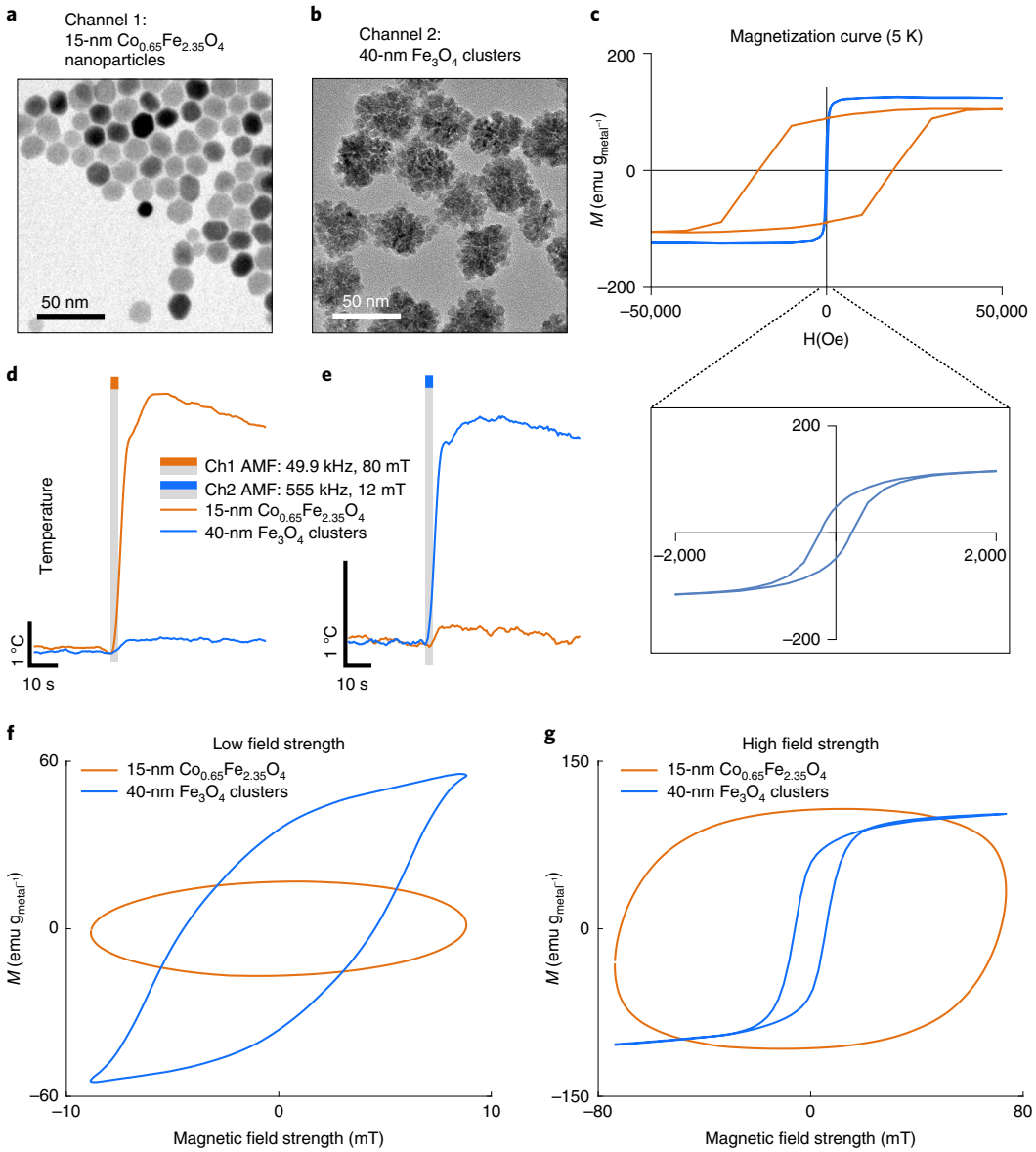

Fig. 4 | Multiplexed magnetothermal heating of nanoparticles. a,**b**, TEM characterization of 15 nm cobalt-doped iron oxide nanoparticles. **b**, TEM characterization of 40 nm iron oxide nanoparticle clusters. TEM images were performed in triplicate, with thousands of particles used to measure average particle diameter. **c**, Superconducting quantum interference device magnetometer data showing high variation in anisotropy between 15 nm cobalt-doped iron oxide (orange) and 40 nm iron oxide clusters (blue), with inset showing more resolved hysteresis loop for low-anisotropy clusters. **d**,**e**, Thermal response of 15 nm cobalt-doped iron oxide nanoparticles (orange, 9.58 mg_{metal} ml^{-1}) and 40 nm iron oxide nanoparticle clusters (blue, 10.09 mg_{metal} ml^{-1}) when exposed to an AMF of 49.9 kHz, 80 mT (**d**) or 555 kHz, 12 mT (**e**). **f**,**g**, Ac magnetometry comparison of hysteresis loops at low (**f**) and high (**g**) field strength at room temperature and 55 kHz. At low field strength (**f**), the open area of the hysteresis loop was greater for 40 nm iron oxide clusters (0.77 mJ g_{metal}^{-1}) than for 15 nm cobalt-doped iron oxide nanoparticles (0.47 mJ g_{metal}^{-1}). However, at high field strength (**g**) the area of cobalt-doped iron oxide nanoparticles (26.21 mJ g_{metal}^{-1}) was greater than that of 40 nm iron oxide nanoparticle clusters (1.78 mJ g_{metal}^{-1}).

FlyTracker metrics was used to train a machine learning model for side-walking behaviour from videos for which side-walking behaviour was hand annotated during thermal activation (35 °C) of flies expressing *dTRPA1-A* under the control of the Hb9-Gal4 driver using the Janelia automated animal behaviour annotator (JAABA)[31]. This model was then used to predict and annotate magnetically stimulated flies for similar behaviour, providing a prediction score. Using FlyTracker and JAABA, we developed a classifier (Methods) to quantify side-walking behaviour before, during and after stimulation. Quantification shows distinct and reversible modulation of side-walking behaviour with iron oxide-injected flies but not with low-SLP SPION-injected control flies (Fig. 3b).

Multiplexed magnetothermal heating in vitro

We next explored whether magnetogenetic stimulation based on rate-sensitive thermoreceptors is compatible with reliable multichannel stimulation. Using nanoparticles that heat at different rates depending on magnetic field conditions, we hypothesized that we could selectively activate flies injected with one type of nanoparticle (channel 1, Ch1) without stimulating flies injected with another type of nanoparticle (channel 2, Ch2), and vice versa. This is analogous to optogenetic stimulation of different neural circuits using different wavelengths of light, but here the selectivity is determined by differences in the SLP of nanoparticles that we design and synthesize. This multiplexing concept is supported by the recent finding that

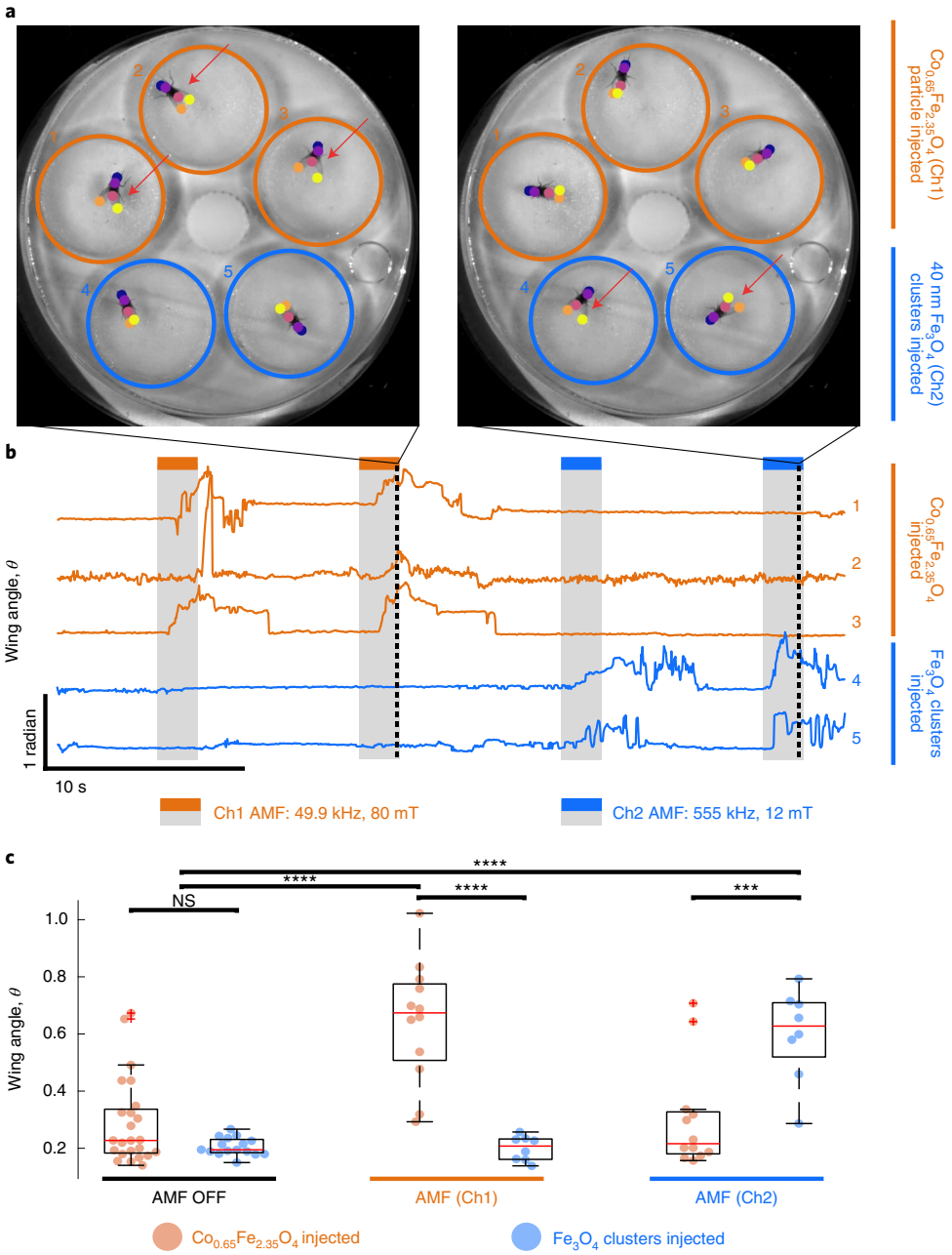

Fig. 5 | Multichannel magnetogenetic stimulation of cells expressing *fruitless*. a, Example images of behaviour chamber containing *Drosophila* with TRPA1-A expressed under the *Fru-Gal4* circuit selectively loaded with individuals injected with 200 nl of either 15 nm cobalt-doped iron oxide (top three chambers, circled in orange) or 40 nm iron oxide clusters (bottom two chambers, circled in blue). Left image was captured during an 80 mT, 49.9 kHz AMF stimulus and shows wing extension of only those flies injected with 15 nm cobalt-doped particles. Right image was captured during a 12 mT, 555 kHz AMF stimulus and shows wing extension of only those flies injected with 40 nm iron oxide clusters. **b**, Wing angle plots tracked by DeepLabCut of five flies exposed to 2 s pulsed magnetic fields (orange: 49.9 kHz, 80 mT; blue: 555 kHz, 12 mT). Top three traces represent flies injected with 200 nl of 15 nm cobalt-doped iron oxide; bottom two traces represent flies injected with 40 nm iron oxide clusters. **c**, Box plots with scatter plots showing the wing angle of each fly immediately before (AMF OFF) and after 2 s of magnetic stimulation (Ch1 and Ch2). $n = 6$ cobalt-injected flies, $n = 4$ nanocluster-injected flies with four repeated AMF stimulations for each channel for each fly. One-way ANOVA (***$P < 0.001$, ****$P < 0.0001$). $P = 1.34 \times 10^{-12}$, $F = 20.08$, d.f. = 5 (Supplementary Video 4). For the box plot, the centre line represents the median with bottom and top edges of the box representing the 25th and 75th percentiles and whiskers extending to extreme data points not considered as outliers.

modulation of the amplitude and frequency of an alternating magnetic field can selectively heat nanoparticles with varying coercivity, resulting in multiplexed magnetothermal heating in vitro[32,33]. One limitation of the magnetic multiplexing modality demonstrated here is that although we can address nanoparticles independently, they activate the same ion channel (TRPA1). This technology is therefore best suited for targeting spatially segregated cell populations, either in different parts of the body or in different animals. The advantage of this type of multiplexing is that we can deliver a magnetic field that penetrates throughout a large volume of tissue (or multiple animals) and yet we can activate different spatially separated neuronal populations by changing magnetic field strength and frequency.

To create the first channel for magnetogenetic heating we developed a highly coercive nanoparticle by doping iron oxide with cobalt ($Co_{0.65}Fe_{2.35}O_4$) (Fig. 4a), which can generate a large amount of heat at a low-frequency AMF with high field strength (Ch1: 80 mT, 49.9 kHz). To create the second channel we used a recently developed iron oxide nanocluster[34] (Fig. 4b) with low coercivity to generate a large amount of heat when exposed to a high-frequency AMF with low field strength (Ch2: 12 mT, 555 kHz). These nanoparticles demonstrate a selectivity of ~15× for cobalt-doped iron oxide nanoparticles in Ch1 (SLP = 829.37 W g^{-1} for cobalt-doped iron oxide, 50.57 W g^{-1} for Fe_3O_4 clusters) and ~10× for iron oxide nanoclusters in Ch2 (SLP = 31.60 W g^{-1} for cobalt, 302.30 W g^{-1} for Fe_3O_4 clusters) when comparing heat generated over 3 s AMF stimulation (Fig. 4d,e), indicating two distinct channels available for magnetothermal heating. Crystal patterns for each particle were confirmed by X-ray power diffraction (XRD), with additional characterization of 19 nm low-SLP SPIONs and 19 nm SPIONs (Supplementary Fig. 4). AC magnetometry further showed how coercivity and saturation differ between particles at relevant temperatures and under AMF conditions (Supplementary Fig. 5). Representative hysteresis loops illustrate how nanoparticle formulation with the largest open hysteresis loop depends on the amplitude of the applied magnetic field. Specifically, we measured areas of 0.77 and 0.47 mJ g_{metal}^{-1} at low field strengths and 1.78 and 26.21 mJ g_{metal}^{-1} at high field strengths for iron oxide clusters and cobalt-doped iron oxide nanoparticles, respectively (Fig. 4f,g). Estimated nanoparticle SLP values from hysteresis loops measured in the double-sided coil varied slightly from measured nanoparticle SLPs in single-coil loops due to the non-uniformity of magnetic fields.

Multiplexed magnetogenetic stimulation in vivo

When we measured wing angle in groups of flies injected with these different nanoparticles, we found that we could selectively drive wing extension in either group depending on which magnetic field stimulation channel was selected. Heating profiles of the nanoparticles were used to scale the concentration of each particle injected into fruit flies to achieve similar heating profiles under each magnetic field condition. We introduced a mixed group of flies injected with cobalt-doped iron oxide (orange circles) or iron oxide nanoclusters (blue circles) into the fly chamber, and showed activation of behaviour specifically in the optimized AMF and lack of a behavioural response under the off-target AMF condition (Fig. 5a–c). Exposure to two stimulations of Ch1 (2 s, 80 mT, 49.9 kHz) followed by two stimulations of Ch2 (2 s, 12 mT, 555 kHz) showed the selectivity on animal behaviour response based on injected particles while maintaining subsecond latencies for each channel (Fig. 5b and Supplementary Video 4).

Outlook

In summary, we report multiplexed magnetothermal activation of behaviour in freely moving adult *D. melanogaster*, and the subsecond magnetogenetic response in vivo. This subsecond response was made possible by replacing the slow-response magnetothermal sensor TRPV1 by a rate-sensitive TRPA1 channel; *Drosophila* TRPA1-A is rate sensitive and native to flies. Magnetic activation of the channel drives behaviour in vivo within 500 ms of stimulation, for which we estimate thermal temperature increases in the tissue to be <1 °C based on nanoparticle heating and the average mass of an adult male *Drosophila* (Methods). Thermal imaging (*FLIR A700*) confirmed neither notable heating of the surface of the fly (Supplementary Fig. 11) nor notable heating of the chamber during magnetic stimulation (Supplementary Fig. 10).

Future applications with targeted nanoparticles may enable multiplexing with similar channels of a heterogeneous population of target neurons or cells within the same volume. However, due to the size of the *Drosophila* nervous system, heat transfer limitations[35] and the thermal rate required to activate these channels to direct behaviour[17], highly concentrated ferrofluids show the most promise for current neuronal stimulation applications. Further sensitization and optimization of thermal rate response may make heterogeneous, multichannel targeted activation of the nervous system possible by genetically targeting nanoparticles to bind to specific membranes or channels.

The ideal magnetothermal sensor for mammalian stimulation at 37 °C may be found among the orthologous TRPA1 proteins in reptilian or avian species and/or through protein engineering, including site-specific mutagenesis or protein chimerization. This new magnetogenetic method depends on *Drosophila* dTRPA1-A, which is constitutively active at 37 °C. To adapt this approach for stimulation of mammalian neurons, other channels with similar temperature rate sensitivities but higher threshold must be characterized or engineered. Reptilian and avian TRPA1 channels have been described as showing a conserved heat response in animals like the western clawed frog, chicken, green anole, rat snake and rattlesnake[36–38], and thus might be promising candidates. These thermal responses have further proven to be heavily reliant on the ankyrin repeat N terminus domain in both *Drosophila* and snakes[17,39], which therefore constitute an ideal target for future protein engineering.

With the relatively fast response and multiplexing abilities of magnetogenetics shown here, we believe that this technology has the potential to rival optogenetics in terms of temporal resolution and multiplexed stimulation while maintaining the advantages of remote activation over large volumes of cells that may lie within deep tissue, such as brain tissue occluded by the skull.

Online content

Any methods, additional references, Nature Research reporting summaries, source data, extended data, supplementary information, acknowledgements, peer review information; details of author contributions and competing interests; and statements of data and code availability are available at https://doi.org/10.1038/s41563-022-01281-7.

Received: 13 March 2021; Accepted: 9 May 2022;
Published online: 27 June 2022

References

1. Huang, H., Delikanli, S., Zeng, H., Ferkey, D. M. & Pralle, A. Remote control of ion channels and neurons through magnetic-field heating of nanoparticles. *Nat. Nanotechnol.* **5**, 602–606 (2010).
2. Munshi, R. et al. Magnetothermal genetic deep brain stimulation of motor behaviors in awake, freely moving mice. *eLife* https://doi.org/10.7554/eLife.27069 (2017).
3. Chen, R., Romero, G., Christiansen, M. G., Mohr, A. & Anikeeva, P. Wireless magnetothermal deep brain stimulation. *Science* **347**, 1477–1480 (2015).
4. Duret, G. et al. Magnetic entropy as a proposed gating mechanism for magnetogenetic ion channels. *Biophys. J.* **116**, 454–468 (2019).
5. Stanley, S. A. et al. Radio-wave heating of iron oxide nanoparticles can regulate plasma glucose in mice. *Science* https://doi.org/10.1126/science.1216753 (2012).
6. Stanley, S. A., Sauer, J., Kane, R. S., Dordick, J. S. & Friedman, J. M. Remote regulation of glucose homeostasis in mice using genetically encoded nanoparticles. *Nat. Med.* **21**, 92–98 (2015).
7. Wheeler, M. A. et al. Genetically targeted magnetic control of the nervous system. *Nat. Neurosci.* **19**, 756–761 (2016).
8. Wang, G. et al. Revaluation of magnetic properties of Magneto. *Nat. Neurosci.* **23**, 1047–1050 (2020).
9. Kole, K. et al. Assessing the utility of Magneto to control neuronal excitability in the somatosensory cortex. *Nat. Neurosci.* **23**, 1044–1046 (2020).
10. Schroll, C. et al. Light-induced activation of distinct modulatory neurons triggers appetitive or aversive learning in *Drosophila* larvae. *Curr. Biol.* **16**, 1741–1747 (2006).
11. Gradinaru, V. et al. Targeting and readout strategies for fast optical neural control in vitro and in vivo. *J. Neurosci.* https://doi.org/10.1523/JNEUROSCI.3578-07.2007 (2007).
12. Liu, Y. et al. Optogenetic study of the response interaction among multi-afferent inputs in the barrel cortex of rats. *Sci. Rep.* **9**, 3917 (2019).

13. Young, J. H. H., Wang, M.-T. T. & Brezovich, I. A. A. Frequency/depth-penetration considerations in hyperthermia by magnetically induced currents. *Electron. Lett.* https://doi.org/10.1049/el:19800255 (1980).
14. Gregurec, D. et al. Magnetic vortex nanodiscs enable remote magnetomechanical neural stimulation. *ACS Nano* **14**, 8036–8045 (2020).
15. Lee, J. et al. Non-contact long-range magnetic stimulation of mechanosensitive ion channels in freely moving animals. *Nat. Mater.* https://doi.org/10.1038/s41563-020-00896-y (2021).
16. Hamada, F. N. et al. An internal thermal sensor controlling temperature preference in *Drosophila*. *Nature* **454**, 217–220 (2008).
17. Luo, J., Shen, W. L. & Montell, C. TRPA1 mediates sensation of the rate of temperature change in *Drosophila* larvae. *Nat. Neurosci.* **20**, 34–41 (2017).
18. Panzano, V. C., Kang, K. & Garrity, P. A. Infrared snake eyes: TRPA1 and the thermal sensitivity of the snake pit organ. *Sci. Signal.* **3**, pe22 (2010).
19. Laursen, W. J., Anderson, E. O., Hoffstaetter, L. J., Bagriantsev, S. N. & Gracheva, E. O. Species-specific temperature sensitivity of TRPA1. *Temp. Multidiscip. Biomed. J.* **2**, 214–226 (2015).
20. Luo, L. et al. Navigational decision making in *Drosophila* thermotaxis. *J. Neurosci.* https://doi.org/10.1523/JNEUROSCI.4090-09.2010 (2010).
21. Rosenzweig, M. et al. The *Drosophila* ortholog of vertebrate TRPA1 regulates thermotaxis. *Genes Dev.* https://doi.org/10.1101/gad.1278205 (2005).
22. Bullock, T. H. & Diecke, F. P. Properties of an infra-red receptor. *J. Physiol.* https://doi.org/10.1113/jphysiol.1956.sp005624 (1956).
23. Inagaki, H. K. et al. Optogenetic control of *Drosophila* using a red-shifted channelrhodopsin reveals experience-dependent influences on courtship. *Nat. Methods* **11**, 325–332 (2014).
24. Dawydow, A. et al. Channelrhodopsin-2–XXL, a powerful optogenetic tool for low-light applications. *Proc. Natl Acad. Sci. USA* **111**, 13972–13977 (2014).
25. von Philipsborn, A. C. et al. Neuronal control of *Drosophila* courtship song. *Neuron* https://doi.org/10.1016/j.neuron.2011.01.011 (2011).
26. Mathis, A. et al. DeepLabCut: markerless pose estimation of user-defined body parts with deep learning. *Nat. Neurosci.* **21**, 1281–1289 (2018).
27. Eyjolfsdottir, E. et al. In *European Conference on Computer Vision* https://doi.org/10.1007/978-3-319-10605-2_50 (2014).
28. Wang, B. et al. Multichannel power electronics and magnetic nanoparticles for selective thermal magnetogenetics. *J. Neural Eng.* **19**, 026015 (2022).
29. Tong, S., Ren, B., Zheng, Z., Shen, H. & Bao, G. Tiny grains give huge gains: nanocrystal-based signal amplification for biomolecule detection. *ACS Nano* https://doi.org/10.1021/nn400733t (2013).
30. Rosenfeld, D. et al. Transgene-free remote magnetothermal regulation of adrenal hormones. *Sci. Adv.* **6**, eaaz3734 (2020).
31. Kabra, M., Robie, A. A., Rivera-Alba, M., Branson, S. & Branson, K. JAABA: interactive machine learning for automatic annotation of animal behavior. *Nat. Methods* https://doi.org/10.1038/nmeth.2281 (2013).
32. Moon, J. et al. Magnetothermal multiplexing for selective remote control of cell signaling. *Adv. Funct. Mater.* **30**, 2000577 (2020).
33. Christiansen, M. G., Senko, A. W., Chen, R., Romero, G. & Anikeeva, P. Magnetically multiplexed heating of single domain nanoparticles. *Appl. Phys. Lett.* **104**, 213103 (2014).
34. Xiao, Z. et al. Libraries of uniform magnetic multicore nanoparticles with tunable dimensions for biomedical and photonic applications. *ACS Appl. Mater. Interfaces* **12**, 41932–41941 (2020).
35. Davis, H. C. et al. Nanoscale heat transfer from magnetic nanoparticles and ferritin in an alternating magnetic field. *Biophys. J.* **118**, 1502–1510 (2020).
36. Saito, S. et al. Analysis of transient receptor potential ankyrin 1 (TRPA1) in frogs and lizards illuminates both nociceptive heat and chemical sensitivities and coexpression with TRP vanilloid 1 (TRPV1) in ancestral vertebrates. *J. Biol. Chem.* https://doi.org/10.1074/jbc.M112.362194 (2012).
37. Saito, S. et al. Heat and noxious chemical sensor, chicken TRPA1, as a target of bird repellents and identification of its structural determinants by multispecies functional comparison. *Mol. Biol. Evol.* https://doi.org/10.1093/molbev/msu001 (2014).
38. Gracheva, E. O. et al. Molecular basis of infrared detection by snakes. *Nature* https://doi.org/10.1038/nature08943 (2010).
39. Geng, J., Liang, D., Jiang, K. & Zhang, P. Molecular evolution of the infrared sensory gene TRPA1 in snakes and implications for functional studies. *PLoS ONE* **6**, e28644 (2011).

Methods

Generation of biocompatible magnetothermal particles. *Superparamagnetic iron oxide nanoparticle synthesis.* Because iron oxide nanoparticles have shown promising biocompatibility[40], we synthesized SPIONs consisting of iron oxide nanocrystals coated with a layer comprising copolymers of phospholipids and poly(ethylene glycol) (DSPE-PEG2K). The nanoparticles were synthesized, coated and functionalized in three consecutive steps similar to previously published work[41]. First, 4 nm iron oxide nanocrystals were synthesized by thermal decomposition of iron acetylacetonate in a mixture of oleic acid and benzyl ether. The iron oxide nanocrystals were then grown to a diameter of 19 nm by controllable seed-mediated growth in a mixture of iron acetylacetonate, oleic acid and benzyl ether. Size distribution of the nanocrystals was then quantified by TEM. The magnetic properties and crystal structure of the nanocrystals were then quantified by a superconducting quantum interference device (SQUID) and power XRD.

The synthesized nanocrystals were then coated with a layer of oleic acid and rendered dispersible in only a non-polar solvent. To generate water-dispersible nanoparticles, nanocrystals were coated with a mixture of DSPE-PEG2K using a dual-solvent exchange method[42]. The hydrodynamic size of conjugated nanoparticles was subsequently examined by dynamic light scattering. The heating efficiency of SPIONs was then examined by magnetic inductive heating within the AMF device using a fiberoptic thermal probe (Lumasense Luxtron 812 and STF-2M Probe).

Cobalt-doped $Co_{0.65}Fe_{2.35}O_4$ nanoparticle synthesis. Cobalt-doped iron oxide nanoparticles were made by multiple seed-mediated growth reactions using 5 nm iron oxide cores. They were synthesized through thermal decomposition, using 2 mmol $CoCl_2$, 4 mmol $Fe(acac)_3$ and 25 mmol oleic acid, and 60 ml of benzyl ether as solvent. The reaction was heated to 120 °C for 30 min under a constant argon flow, then to 200 °C for 2 h and finally to reflux at 300 °C for 30 min. The product was purified through several acetone washes. Nanoparticle size was determined by high-contrast TEM (JEOL JEM-1230), and they were then coated with DSPE-PEG2K by mixing with PEG and the addition of DMSO. The reaction was then evaporated and transferred to water by dropwise addition of water, with removal of the remaining DMSO by centrifugation and ultracentrifugation.

Iron oxide nanocluster (40 nm) synthesis. The 40 nm iron oxide nanocrystal clusters were synthesized by hydrothermal reaction. $FeCl_3{\cdot}6H_2O$ (540 mg) was dissolved in ethylene glycol (20 ml) under vigorous magnetic stirring, then poly(acrylic acid) (250 mg), urea (1,200 mg) and ultrahigh-purity deionized water (1.0 ml, <18 mΩ) were added to the solution. The mixture was vigorously stirred for 30 min, yielding a transparent, bright yellow solution. The mixture was then transferred to a Teflon-lined stainless steel autoclave, tightly sealed and heated at 195 °C for 6 h at a temperature ramp rate of 20 °C min^{-1}. After cooling of the reaction mixture to room temperature, the product was collected using a magnet. Clusters were washed six times using ethanol and water to remove unreacted reactants and byproducts, then dispersed in deionized water. Sizes of clusters and primary particles were determined using TEM, with >500 clusters measured to determine cluster dimensions.

Low-SLP SPION nanoparticle synthesis. Synthesis of control low-SLP SPION nanocrystals, which are poor magnetothermal transducers, was achieved similarly to SPION synthesis with minor alterations. Benzyl ether was substituted with oleylamine, the initial reaction was lengthened by reduced temperature and a vacuum process was added. Low-SLP SPION nanocrystals were then purified with ethanol, surface treated by heating in oleylamine and dispersed in toluene before coating with DSPE-PEG2K.

Samples for TEM measurement, by both HC TEM and Titan TEM, were prepared by dilution followed by placing them in carbon-film grids. XRD samples were prepared by drying nanoparticles under an argon flow and then pulverizing the resulting powder. SQUID measurements were carried out with coated samples by fixing the nanoparticles with calcium hemisulfate and enclosing them within a capsule to prevent movement, followed by normalization in terms of metal as determined by ferrozine assay and inductively coupled mass spectrometry (ICP–MS). Doping percentages were determined by ICP–MS and samples compared to the corresponding standard curves of iron and cobalt. SLP was calculated thus:

$$\mathrm{SLP} = C(\Delta T/\Delta t)\rho^{-1} \quad (1)$$

where C is the specific heat capacity of the medium (4,180 J kg^{-1} K^{-1}), T is the total temperature change during stimulation averaged over three stimulations, t is the AMF stimulation time and ρ is the sample density as measured by total metal concentration. Iron oxide nanoclusters and cobalt-doped iron oxide nanoparticles were recorded at 10.09 and 9.58 mg_{metal} ml^{-1}, respectively. Temperature was measured with a fiberoptic thermal probe (Lumasense Luxtron 812 and STF-2M Probe), which is unaffected by magnetic field.

Fly stocks and husbandry. Parental *Drosophila* strains were either a gift from the Venkatachalam laboratory (strain UAS-hTRPV1 P{w[+mC]=UAS-VR1E600K}, generated by random P-element insertion and mapped to the second chromosome)[43]

or acquired from the Bloomington Drosophila Stock Center:

Fru-GAL4 (BL66696) w[*]; TI{GAL4}fru[GAL4.P1.D]/TM3, Sb[1] (ref. [44])

UAS-TrpA1-A (BL26263) w[*]; P{y[+t7.7] w[+mC]=UAS-TrpA1(B).K} attP16 ([45])

Hb9-GAL4 (BL32555) w[*]; P{w[+mW.hs]=GawB}exex[Gal4] P{w[+mC]=lacW}nsl1[S009413]/TM3, P{w[+mC]=GAL4-Kr.C}DC2, P{w[+mC]=UAS-GFP.S65T}DC10, Sb[1] (ref. [46]).

All flies were reared on cornmeal, molasses, sugar, yeast and agar food, on a 16/8 h light/dark cycle at room temperature (22.5 ± 0.5 °C).

Nanoinjection of nanoparticles into the *Drosophila* head. Different *GAL4* driver lines were crossed with *UAS-TRPA1* flies and offspring with both *GAL4* and *UAS* components, and single-component controls were collected for injection. Nanoparticles were injected into adult male heads similarly to a previously described protocol[47]. Males aged 1–5 days were immobilized on ice and dropped head-down with an aspirator into a cylindrical hole, punched with a Pasteur pipette tip, into a 2% ice-cooled agarose gel (approximately 5 mm thick). The flies were then aspirated through the gel until the top of the head was flush with the gel surface. Five flies were immobilized simultaneously in a gel and transferred to a thermoelectric temperature controller (TE Technology). Using a Nanoject II (Drummond Scientific) and a borosilicate needle pulled on a Model P-97 needle puller (Sutter Instruments), nanoparticles resuspended in artificial *Drosophila* haemolymph[47] were aspirated into the needle. Using a micromanipulator (Narishige, no. M-152) attached to a fixed post to move the Nanoject in three dimensions, the needle tip was placed just above the top of the fly head protruding from the refrigerated gel and positioned between the three ocelli at an angle of 45°. Flies were then injected by gently pushing the needle forward until it penetrated the cuticle between the ocelli. Approximately 200 nl of nanoparticles suspended in artificial haemolymph was injected directly into the brain, and flies were aspirated through the gel into an empty vial containing standard fly food. Iron oxide nanoparticles of diameter 19 nm were injected at 10 mg ml^{-1}, cobalt-doped iron oxide particles were injected at 10 mg ml^{-1} and 40 nm iron oxide clusters injected at 25 mg ml^{-1}. Flies were then allowed to recover overnight before being placed in a behaviour chamber and stimulated with AMF (Fig. 1).

AMF stimulation of *Drosophila*. Flies were given at least 16 h to recover from nanoparticle injection before loading into the AMF generator. Experimental and control flies were placed in one of five cylindrical arenas (12 mm diameter) in the behavioural chambers within a 50-mm-diameter enclosure, by aspiration through a small hole cut into an acrylic cover that can rotate over each arena. This three-dimensional (3D) printed behaviour chamber was then placed in a 3D printed chamber holder, which places the flies in the centre of either (1) a 17 turn, 50-mm-inner diameter (ID) coil (Nanotherics Magnetherm) for courtship behaviour using 19 nm SPIONs (Supplementary Fig. 2) or (2) a custom high-powered six-turn 50-mm-ID coil (Fluxtrol/AMF Lifesystems) for side-walking behaviour experiments via inductive heating. Stimulation of cobalt nanoparticles and iron oxide nanoclusters was performed by placing the chamber ~6 mm above the surface of a six-turn, 57.7-mm-ID Hi-Flux coil with a ferrite core (μ = 2,300) (MSI Automation) driven by a custom field-programmable gate array controlled hybrid silicon–gallium nitride transistor-based power electronics system (Duke University), which can generate AMF in the same coil at several distinct frequency channels spanning 50 kHz to ~5 MHz and rapidly switch between channels on a millisecond time scale. The camera (Basler acA2000-165 µm NIR, 50 mm F1.8 Edmund optics 86574) was then fixed above the flies and synchronized with the AMF by through-the-lens triggers to temporally align behavioural recordings with magnetic field generation. Frequency was set by the machine, while field strength was measured by a magnetic field probe placed in the same location as the fly behaviour chamber (Fluxtrol).

Thermal ramp demonstration used two stimulations of 1.8 s duration at 80 mT and 49.9 kHz for rapid heating, and 20 s duration at 19 mT and 49.9 kHz for slow heating. Interstimulation intervals were 30 and 60 *s* for rapid and slow heating, respectively. Multichannel demonstration used exposure to two stimulations of Ch1 (2 s, 80 mT, 49.9 kHz) followed by two stimulations of Ch2 (2 s, 12 mT, 555 kHz), with an interstimulation interval of 10 s. Video recording was paused for <1 s in the multiplexing recording (t = 20 *s*) to switch the stimulation protocol on the software from Ch1 to Ch2.

Automated analysis of behavioural phenotypes in *Drosophila*. Flies were given at least 5 min to adjust to the behaviour chamber before stimulation with pulsed cycles of alternating magnetic fields. Backlit videos of flies were analysed using Caltech FlyTracker[27] to automatically identify position, orientation and wing/leg extensions. These data were then analysed on a frame-by-frame basis in MATLAB (MathWorks) for specific phenotypes (for example, maximum wing angle for wing extension phenotype and position for side-walking phenotype) or used with machine learning tools such as JAABA to train complex behaviours that take place over a series of frames (lateral movement phenotype in side-walking), which enables prediction by linear regression models of the occurrence of that phenotype.

Multiplexed animal behaviour was analysed using DeepLabCut[26] for dynamic tracking of flies with visible shadows introduced by frontlighting to illuminate individuals above the ferrite core. Animal analysis was trained using a skeleton labelling the head, neck, tip of each wing and abdomen. Wing angle was calculated between the neck and each wingtip.

Each experiment consisted of two AMF stimulations per fly and was repeated twice per fly. Experiments were performed on a minimum of 20 flies for control groups and on 40 for those expressing TRPA1 under the *fruitless* driver. Traces were sorted by average area under curve during magnetic stimulation, and the top ten flies from each group were used to calculate comparisons from control versus experimental groups (Supplementary Figs. 6 and 7) while the top 20 were used to compare across conditions for flies expressing TRPA1 under the *fruitless* driver (Fig. 2). The selection of the most responsive ten or 20 flies from each group was done to remove data from individuals that were poorly injected, which is a known challenge related to backflow of the nanoparticle solution. Additionally, this selection process eliminates data with DeepLabCut tracking errors. Power analysis performed with G*power on an average of five flies suggested that a sample size of $n=5$ is sufficient for experimental versus control groups, and $n=8$ is sufficient for thermal rate comparisons against controls (Supplemetary Fig. 8).

Side-walking and multiplexing experiments were done with fewer flies, because these experiments show extensions of the basic experimental approach. Statistics for Fig. 3b are shown for each stimulation with $n=15$ flies (nine injected with SPIONs and six with low-SLP SPIONs, and two repeated stimulations per fly). Statistics for Fig. 5c are shown as individual simulations of each fly: $n=6$ cobalt-injected and $n=4$ nanocluster-injected, with four repeated stimulations for each channel per fly.

Thermal imaging of fly chamber and immobilized flies. To assess the thermal stability of the chamber during magnetic stimulation, the chamber was located above the magnet without the acrylic lid to enable thermal imaging of the interior of the chamber. Previously injected flies expressing TRPA1 under the control of the *fruitless* gene and that were shown to be responsive were immobilized and placed in the chamber. Thermal imaging (FLIR A700) was performed on the chamber and flies to verify ambient heat. Regions of interest were traced around the flies and analysed using the manufacturer's software (FLIR research studio). Raw traces of individual chambers without flies under magnetic stimulation are shown in Supplementary Fig. 10, and fly heating data are shown by subtracting the temperature of a nearby area within the chamber without an injected fly to offset baseline fluctuations introduced from the camera sensor (Supplementary Fig. 11).

Theoretical calculation of thermal fluctuation in injected *Drosophila*. To determine the thermal fluctuation of fly tissues during magnetic stimulation, we use the density-based SLP of the nanoparticles (equation (2)) to estimate the change in fly tissue temperature based on their mass, using a simple mass dilution (equation (3)). Heat flux exiting the fly is assumed to be negligible compared with that dissipated by particles, because no heating of the fly surface was visible with infrared imaging (Supplementary Figs. 10 and 11). For this measurement we assume the mass of the adult male fruit fly is ~0.88 mg, as previously shown[48], with a specific heat capacity in the range 70–100% that of water (4,180 J kg^{-1} K^{-1}) (equation (4)):

$$\mathrm{SLP} = C(\Delta T/\Delta t)\rho^{-1} = 829.37\ \mathrm{W\ g^{-1}} \tag{2}$$

$$\begin{aligned}&\text{Sample dilution (Mass/Mass)} = V_{\text{NP Injection}}\rho_{\text{NPs}}(M_{Drosophila})^{-1}\\&\text{Sample dilution} = (200\ \text{nl}\ 10\ \text{mg ml}^{-1})\ (0.88\ \text{mg}_{\text{fruitfly}})^{-1} \approx 1/4.4\end{aligned} \tag{3}$$

$$\begin{aligned}\Delta T_{Drosophila} &= (\mathrm{SLP_{NPs}}\ \rho_{\mathrm{NPs}}\ \Delta t\ C^{-1})\ (\text{Sample dilution})\\ \Delta T_{Drosophila} &= \big(829.37\ \mathrm{W\ g^{-1}}\ 10.09\ \mathrm{mg\ ml^{-1}}\\ &\quad 1.8\ \mathrm{s}\ (4,180\ \mathrm{J\ kg^{-1}\ K^{-1}})^{-1}\big)\ (1/4.4) \approx 0.82\ ^{\circ}\mathrm{C}\\ \Delta T_{Drosophila} &= \big(829.37\ \mathrm{W\ g^{-1}}\ 10.09\mathrm{mg\ ml^{-1}}\\ &\quad 1.8\ \mathrm{s}\ (0.7\times 4,180\ \mathrm{J\ kg^{-1}\ K^{-1}})^{-1}\big)\ (1/4.4) \approx 1.17\ ^{\circ}\mathrm{C}\end{aligned} \tag{4}$$

Because this calculation relies on assumptions of the thermal capacitance (C) of each fly being ~70–100% that of water, we expect that flies in all experiments received the same total heat but at different rates ($\Delta T = C/Q$). As such, we simply estimate an upper bound of ~1.17 °C overall change in the temperature of bulk fly tissue and show how this temperature may adjust with a sliding specific heat capacity ranging 70–100% that of water (Supplementary Fig. 12). Because nanoparticle distribution may be localized within areas of the fly, it is possible that these areas may reach slightly higher temperatures; however, because flies can tolerate a change of several degrees in temperature, we can reasonably rule out damage from magnetic hyperthermia.

Alternating current measurement of nanoparticle dynamic magnetization. A custom double-sided, high-amplitude AMF generator was constructed from superconductive copper tubing (10 AWG equivalent) and two E-shaped, N87 ferrite cores ($\mu=2{,}200$; TDK Electronics). The cores were each wrapped by nine turns then assembled with material between the outside arms to create an air gap of 5.3 mm between the middle arms. The two coils and a resonant capacitor were wired in series, and the circuit was driven by a custom air-cooled gallium nitride transistor-based power electronics board (Duke University). This driver board consisted of an H bridge powered by a voltage-controlled direct current power supply (Aim-TTI QPX1200S) and gated by a two-channel function generator (BK Precision, no. 4052).

A 17 µl sample of nanoparticles (~10 mg ml^{-1}) suspended in water was loaded into a 3D printed, hollow chamber. The chamber was sealed with Scotch tape and placed on a custom two-layer, 16-mm-thick ac magnetometer (ACM) circuit board (MIT)[32]. The ACM board was then positioned within the AMF generator air gap such that the field was completely uniform across the board's two oppositely wound inductive pickup coils (one containing the sample and the other empty). Field strength measurements from the circuit board's single-turn pickup coil were calibrated with a high-frequency magnetic field probe (Fluxtrol). At each field strength, the AMF generator was driven for 200 ms at 55 kHz and the final 100 periods of signals induced by the applied AMF and changing nanoparticle magnetization were captured, filtered and amplified on the ACM board. The same protocol was run with 17 µl of water in the sample chamber.

Magnetization signals from the nanoparticle and water samples were subtracted to further reduce noise and isolate true nanoparticle magnetization. The resulting voltage signals were integrated to yield AMF and nanoparticle dynamic magnetization signals. Magnetization was normalized with respect to sample concentration, then calibrated by setting the saturation magnetization to that measured by SQUID. The 100 collected periods were each centred and the average taken across all periods to yield the average hysteresis loop.

Statistics and reproducibility. Sample sizes were calculated using G*Power using preliminary data from five flies in each group (control versus experimental). Sample sizes were calculated using analysis of variance (ANOVA): fixed effects, omnibus, one-way test with an alpha error probability of 0.05 and power of 0.8. The two-group test was conducted with fast ramp data versus uninjected controls only, resulting in an effect size of $f=2.12$; the three-group test was conducted comparing fast and slow ramp data versus uninjected controls, resulting in an effect size of $f=1.56$. This confirmed that a sample size of five or more would be adequate for experimental versus control, and eight or more would be sufficient for comparison of slow versus fast ramps and controls. We exceeded this and used ten flies for comparison against control and 20 experimental flies for comparison between the different thermal ramp conditions. Reproducibility and details of data exclusion are provided in Automated analysis of behavioural phenotypes in Drosophila.

Reporting summary. Further information on research design is available in the Nature Research Reporting Summary linked to this article.

Data availability

The main data supporting the results of this study are available within the paper and its Supplementary information. The raw videos generated for the study are too large for public sharing, but are available for research purposes from the corresponding authors upon reasonable request.

Code availability

FlyTracker (Perona Lab, CalTech, v.1.0.5) was used to track the wing angle and position of flies within their respective chambers, and is publicly available online (https://www.vision.caltech.edu/datasets/). DeepLabCut (Mathis Lab, v.2.2.b9) was used to track fly wing angle and position for videos with shadows, and is publicly available online (http://www.mackenziemathislab.org/deeplabcut). Microsoft excel (v.16.54) was used for simple SLP and selectivity calculations. FLIR research studio (v.2.0) was used for thermal imaging.

References

40. Hanini, A. et al. Evaluation of iron oxide nanoparticle biocompatibility. *Int. J. Nanomed.* **6**, 787–794 (2011).
41. Tong, S., Quinto, C. A., Zhang, L., Mohindra, P. & Bao, G. Size-dependent heating of magnetic iron oxide nanoparticles. *ACS Nano* https://doi.org/10.1021/acsnano.7b01762 (2017).
42. Tong, S., Hou, S., Ren, B., Zheng, Z. & Bao, G. Self-assembly of phospholipid-PEG coating on nanoparticles through dual solvent exchange. *Nano Lett.* https://doi.org/10.1021/nl201978c (2011).
43. Marella, S. et al. Imaging taste responses in the fly brain reveals a functional map of taste category and behavior. *Neuron* **49**, 285–295 (2006).
44. Stockinger, P., Kvitsiani, D., Rotkopf, S., Tirián, L. & Dickson, B. J. Neural circuitry that governs *Drosophila* male courtship behavior. *Cell* **121**, 795–807 (2005).
45. Kang, K. et al. Modulation of TRPA1 thermal sensitivity enables sensory discrimination in *Drosophila*. *Nature* **481**, 76–80 (2011).

46. Broihier, H. T. & Skeath, J. B. *Drosophila* homeodomain protein dHb9 directs neuronal fate via crossrepressive and cell-nonautonomous mechanisms. *Neuron* **35**, 39–50 (2002).
47. Lima, S. Q. & Miesenböck, G. Remote control of behavior through genetically targeted photostimulation of neurons. *Cell* **121**, 141–152 (2005).
48. Dierick, H. A. & Greenspan, R. J. Molecular analysis of flies selected for aggressive behavior. *Nat. Genet.* **38**, 1023–1031 (2006).

Acknowledgements

This research was developed with funding from the Defense Advanced Research Projects Agency of the United States of America (contract no. N66001-19-C-4020, received by J.T.R.). The views, opinions and/or findings expressed are those of the authors and should not be interpreted as representing the official views or policies of the Department of Defense or the US Government. This work was funded in part by the National Science Foundation: Neuronex innovation award no. 1707562 and grant no. C-1963 from the Welch Foundation received by J.T.R., as well as by the National Institutes of Health under award no. RO1MH107474 received by H.A.D. We thank J. Moon and P. Anikeeva (MIT) for useful discussions and guidance with magnetic multiplexing, sharing their design for the ac magnetometer and advising us on its operation.

Author contributions

C.S. designed, performed and analysed the in vivo behavioural assays for *Drosophila*. D.T.H. synthesized, coated, functionalized and characterized iron oxide nanoparticles and low-SLP and cobalt-doped nanoparticles. K.J. prepared nanoparticles for testing and L.Z. assisted with heating measurements. Z.X. and Q.Z. synthesized and characterized iron oxide nanoclusters. C.S. and D.T.H. recorded SLP measurements of nanoparticles and nanoclusters. C.S. and H.A.D. designed and performed the nanoparticle injection scheme for adult *Drosophila*. B.W. and Z.L. designed and built the custom AMF system used for in vivo recordings and the magnetic field driver used for the ac magnetometer. J.A. built the ac magnetometer and recorded dynamic hysteresis loops. C.S. and J.A. performed thermal imaging experiments. J.T.R., H.A.D. and G.D. contributed to the design of the experiments. H.A.D. and J.T.R. supervised behavioural assay design and development. S.M.G. and A.V.P. supervised AMF system design and development. V.L.C. and G.B. supervised nanoparticle synthesis, characterization and functionalization. C.S., D.T.H., B.W., J.A., J.T.R. and H.A.D. prepared the manuscript with input from all authors.

Competing interests

The authors declare the following competing interests. S.M.G. has received research funding from Magstim. A.V.P. has received research funding, travel support, patent royalties, consulting fees, equipment loans, hardware donations and/or patent application support from Rogue Research, Tal Medical/Neurex, Magstim, MagVenture, Neuronetics, BTL Industries and Advise Connect Inspire. The remaining authors declare no competing interests.

Additional information

Supplementary information The online version contains supplementary material available at https://doi.org/10.1038/s41563-022-01281-7.

Correspondence and requests for materials should be addressed to Jacob T. Robinson.

Peer review information *Nature Materials* thanks Michael Christiansen, Andre Fiala and the other, anonymous, reviewer(s) for their contribution to the peer review of this work.

nature research

Corresponding author(s): Jacob T Robinson

Last updated by author(s): Apr 4, 2022

Reporting Summary

Nature Research wishes to improve the reproducibility of the work that we publish. This form provides structure for consistency and transparency in reporting. For further information on Nature Research policies, see our Editorial Policies and the Editorial Policy Checklist.

Statistics

For all statistical analyses, confirm that the following items are present in the figure legend, table legend, main text, or Methods section.

n/a	Confirmed	
☐	☒	The exact sample size (*n*) for each experimental group/condition, given as a discrete number and unit of measurement
☐	☒	A statement on whether measurements were taken from distinct samples or whether the same sample was measured repeatedly
☐	☒	The statistical test(s) used AND whether they are one- or two-sided *Only common tests should be described solely by name; describe more complex techniques in the Methods section.*
☒	☐	A description of all covariates tested
☒	☐	A description of any assumptions or corrections, such as tests of normality and adjustment for multiple comparisons
☐	☒	A full description of the statistical parameters including central tendency (e.g. means) or other basic estimates (e.g. regression coefficient) AND variation (e.g. standard deviation) or associated estimates of uncertainty (e.g. confidence intervals)
☐	☒	For null hypothesis testing, the test statistic (e.g. *F*, *t*, *r*) with confidence intervals, effect sizes, degrees of freedom and *P* value noted *Give P values as exact values whenever suitable.*
☒	☐	For Bayesian analysis, information on the choice of priors and Markov chain Monte Carlo settings
☒	☐	For hierarchical and complex designs, identification of the appropriate level for tests and full reporting of outcomes
☒	☐	Estimates of effect sizes (e.g. Cohen's *d*, Pearson's *r*), indicating how they were calculated

Our web collection on statistics for biologists contains articles on many of the points above.

Software and code

Policy information about availability of computer code

Data collection	Videos were captured using Image acquisition toolbox in Matlab R2020b supported by Basler pylon GenTL. Thermal imaging data was aquired using FLIR Research Studio (2.0)
Data analysis	FlyTracker (CalTech - Version 1.0.5) used to track wing angle and position of flies within their respective fly chamber. DeepLabCut (Mathis Lab - Version 2.2.b9) used to track wing angle and position of flies for videos with shadows. Analysis and plots made in matlab R2020b. Microsoft excel (Version 16.54) was used for simple SAR and selectivity calculations. FLIR Research Studio (V2.0) was used for thermal imaging.

For manuscripts utilizing custom algorithms or software that are central to the research but not yet described in published literature, software must be made available to editors and reviewers. We strongly encourage code deposition in a community repository (e.g. GitHub). See the Nature Research guidelines for submitting code & software for further information.

Data

Policy information about availability of data

All manuscripts must include a data availability statement. This statement should provide the following information, where applicable:

- Accession codes, unique identifiers, or web links for publicly available datasets
- A list of figures that have associated raw data
- A description of any restrictions on data availability

The data that support the findings of this study are available from the corresponding author upon reasonable request as raw video files are too large to be easily uploaded into a repository.

Field-specific reporting

Please select the one below that is the best fit for your research. If you are not sure, read the appropriate sections before making your selection.

☒ Life sciences ☐ Behavioural & social sciences ☐ Ecological, evolutionary & environmental sciences

For a reference copy of the document with all sections, see nature.com/documents/nr-reporting-summary-flat.pdf

Life sciences study design

All studies must disclose on these points even when the disclosure is negative.

Sample size	We conducted the experiment on sample size (N=5) for 2x repeated protocols of 2x stimulations for each stimulation type. The responses were significant when compared to control for each fly under each experimental case resulting in one-sided ANOVA results with confidence intervals > 99.9% for each study.
Data exclusions	Some experimental animals were excluded from study based on unsuccessful injection resulting in back-flow of nanoparticle ferrofluid.
Replication	Stimulation protocols were replicated 2x per experimental recording and then performed again on the same set of animals indicating reproducibility.
Randomization	Experimental drosophila of the F1 generation were randomly split into group for injection with different particle types or no particle injection before performing experiments.
Blinding	Data analysis was automated with animal tracking software like DLC and Flytracker and was not influenced by the experimenting scientist. Experimenters were not blinded as the automated analysis enabled unbiased quantification of behavioral responses.

Reporting for specific materials, systems and methods

We require information from authors about some types of materials, experimental systems and methods used in many studies. Here, indicate whether each material, system or method listed is relevant to your study. If you are not sure if a list item applies to your research, read the appropriate section before selecting a response.

Materials & experimental systems

n/a	Involved in the study
☒	☐ Antibodies
☒	☐ Eukaryotic cell lines
☒	☐ Palaeontology and archaeology
☐	☒ Animals and other organisms
☒	☐ Human research participants
☒	☐ Clinical data
☒	☐ Dual use research of concern

Methods

n/a	Involved in the study
☒	☐ ChIP-seq
☒	☐ Flow cytometry
☒	☐ MRI-based neuroimaging

Animals and other organisms

Policy information about studies involving animals; ARRIVE guidelines recommended for reporting animal research

Laboratory animals	Parental Drosophila melanogaster strains were obtained from the Bloomington Drosophila Stock Center: Fru-GAL4 (BL66696), UAS-TrpA1-A (BL26263), Hb9-GAL4 (BL32555). Experiments were performed on F1 1-5 day old male flies of all possible genotypes.
Wild animals	No wild animals were used in the study.
Field-collected samples	No field collected samples were used in the study.
Ethics oversight	The study did not require ethical oversight or approval.

Note that full information on the approval of the study protocol must also be provided in the manuscript.